RSC Advances

PAPER

View Article Online
View Journal | View Issue

Cite this: *RSC Adv.*, 2024, **14**, 12323

Selenosalicylate; a little-studied heavy-element analogue of the versatile thiosalicylate ligand†

Simeon Atiga, *[ab] Graham C. Saunders [a] and William Henderson [a]

Received 5th February 2024
Accepted 2nd April 2024

DOI: 10.1039/d4ra00926f

rsc.li/rsc-advances

Selenosalicylic acid (*ortho*-$HSeC_6H_4CO_2H$), the heavy element congener of the widely studied thiosalicylic acid, was prepared by reaction of 2-carboxybenzenediazonium chloride ($HO_2CC_6H_4N_2^+Cl^-$) with Na_2Se_2, followed by reduction of the resulting diselenide $(SeC_6H_4CO_2H)_2$ with zinc and acetic acid. The coordination chemistry of the selenosalicylate ligand towards a variety of platinum(II), palladium(II), nickel(II), gold(III), gold(I), rhodium(III), iridium(III) and ruthenium(II) centres was explored. X-ray crystal structure determinations were carried out on the complexes $[Pt(SeC_6H_4CO_2)(PPh_3)_2]$, $[\{(p\text{-cym})Ru(SeC_6H_4CO_2)\}_2]$ (*p*-cym = η^6-*p*-cymene, $CH_3C_6H_4CH(CH_3)_2$), $[\{Cp^*Rh(SeC_6H_4CO_2)\}_2]$ (Cp^* = η^5-C_5Me_5) and $[Cp^*Ir(SeC_6H_4CO_2)(PPh_3)]$, and comparisons are made with corresponding thiosalicylate complexes. The complexes were characterised by NMR spectroscopy as well as ESI mass spectrometry, which indicated a greater propensity for fragmentation including by selenium loss, compared to the thiosalicylate analogues. Hirshfeld surface analysis to visualise and quantify intermolecular interactions revealed the dominance of H···H contacts in $[\{(p\text{-cym})Ru(SeC_6H_4CO_2)\}_2]$ and $[Cp^*Ir(SeC_6H_4CO_2)(PPh_3)]$.

Introduction

The thiosalicylate ligand, derived by deprotonation of thiosalicylic acid **1**, is an interesting heterodifunctional ligand containing both soft thiolate and hard carboxylate donors. Thiosalicylate forms coordination complexes with a diverse range of metals from across the periodic table, as well as finding applications in materials chemistry, and the coordination chemistry of this ligand has been reviewed.[1] In contrast, little is known about the analogous selenosalicylate ligand, derived from selenosalicylic acid **2**.

Selenium-containing compounds are important because Se is an essential trace element and possesses physiological functions effectuated by its incorporation into selenoproteins containing selenocysteine.[2] Proteins containing selenium show more reactivity than corresponding sulfur derivatives[3] and are highly effective in catalysis compared to their cysteine homologs,[4] thus playing important roles in thyroid metabolism, inflammation, the aging process, immune defense, and redox state regulation.[5–8] Selenoprotein-mediated bioprocesses play central roles in the prevention, onset, and modulation of the clinical outcome of cardiovascular, neurological, and mental disorders, fertility impairment, infections, diabetes, and cancer.[8,9] Following these, research in synthetic selenium compounds has been used to identify various areas of application despite associated toxicity concerns.[10] For example, synthesised 2-phenyl-1,2-benzisoselenazol-3(2*H*)-one (ebselen) is capable of mimicking the catalytic activities of glutathione peroxidases[11] and also has antioxidant and anti-inflammatory properties.[12] Related small-molecule mimics include ebselen-appended β-cyclodextrins,[13] phenylselenenyl-1-naphthol,[14] selenium-containing analogues of known anti-oxidants[15,16] and carbohydrates,[17] and cyclic seleninate esters.[18,19] Biologically active organoselenium compounds[20–25] are categorised into cyclic selenyl amides bearing Se–N bonds, diaryldiselenides, and monoselenides with aryl or alkyl substituents.[26–28] Se-containing compounds have been reported to demonstrate synergistic effects in combination with other therapeutic compounds,[29,30] including metal complexes,[31] and also act as biosensing materials in probe design.[32] Similarly, inorganic species such as sodium selenite ($NaSeO_3$), sodium selenate ($NaSeO_4$) and sodium selenosulfate ($NaSeSO_3$) have been reported to possess activity toward cancer.[33]

Selenolate ligands have been reported to coordinate with metals. For example, quinoline-8-selenol was reacted with metal salts to generate the Zn, Cd, Hg, Ga, In, Sn, Pb, As, Sb, Bi, V, Mo, Cr, Ag, Pd, Pt, Ir, Ru, and Os compounds[34] although detailed characterisation data were not reported. A variety of Pt and Pd selenolates have also been prepared from different stoichiometric combinations of $[M_2Cl_2(\mu\text{-}Cl)_2(PR_3)_2]$ (PR_3 = PEt_3, P^nPr_3, and PMe_2Ph) and $MeO(O{=}C)CH_2CH_2SeNa$ where the ligand formed bridges between metal centres.[35] Similarly, the sodium salt of a selenopyrimidine has been reported to exhibit both Se

[a]*Chemistry, School of Science, University of Waikato, Private Bag 3105, Hamilton 3240, New Zealand. E-mail: simeon.atiga@waikato.ac.nz*

[b]*Department of Chemistry, Faculty of Natural Sciences, Kogi State University, PMB 1008, Anyigba, Kogi State, Nigeria*

† Electronic supplementary information (ESI) available. CCDC 2211290–2211293. For ESI and crystallographic data in CIF or other electronic format see DOI: https://doi.org/10.1039/d4ra00926f

and Se,N coordination with platinum and palladium as in $[Pt(SeC_4H_3N_2)_2(PPh_3)_2]$ and $[Pd\{\eta^2\text{-}SeC_4H_3N_2\}\{SeC_4H_3N_2\}(PPh_3)]$.[36] The phenylselenolate ligand (–SePh) and its phenyl-substituted derivatives, usually furnished by cleaving the –Se–Se– bond of their respective diselenides, have a predominant presence in the literature and have been observed in complexes across different groups of metals.[37–39] The ability of selenoamino acids to act as a good metal ligand is important in the binding of toxic heavy metals in the body.[40,41] The selenol group (–SeH) in selenocysteine is more acidic than the thiol group (–SH) ($pK_{thiol} \sim 8.5$ and $pK_{selenol} \sim 5.2$)[42] and is deprotonated at physiological pH,[43] making metal binding feasible. A study of the binding properties of selenocysteine with Hg, Cd, Zn, Ni and Co demonstrated that one M^{2+} binds to one SeCys to form a stable M(SeCys) complex with a binding constant order of $Hg^{2+} > Cd^{2+} \sim Zn^{2+} > Ni^{2+} > Co^{2+}$.[42] Platinum and palladium square-planar complexes of selenomethionine (SeMet) have also been synthesised and characterised spectroscopically.[44,45] The antiproliferative, antibacterial and antifungal potentials of different complexes based on selenium ligands and some transition metals was reviewed by Ramos-Inza *et al.*[33] Other properties of selenium complexes with possible applications include their semiconducting and sensing behaviours.[46,47]

The only selenium-coordinated selenosalicylate complexes are the analogues of the well-known antibacterial Thiomersal $EtHgSC_6H_4CO_2Na$, *viz.* $RHgSeC_6H_4CO_2H$ (R = Et or *n*-Pr).[48] The dinuclear carboxylate-bridged copper(II) complex $[Cu_2(\mu\text{-}O_2CC_6H_4SeH)_4(EtOH)_2]$ has also been reported.[49,50] In general, the coordination chemistry of selenolates[51] is less developed when compared to their thiolate counterparts, due to a combination of the higher toxicity, more disagreeable stench, and greater air-sensitivity of selenols, RSeH.[52] Despite this, selenium-containing ligands do offer some advantages such as the accessibility of an NMR active isotope (^{77}Se, I = $\frac{1}{2}$, 7.6% abundance).

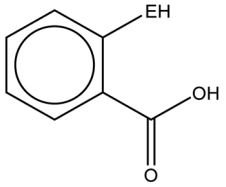

1 E = S
2 E = Se

In this contribution, the coordination chemistry of the selenosalicylate ligand is explored, and the structural properties of related complexes of thiosalicylate and selenosalicylate are compared. This provides the opportunity to understand any difference in coordination chemistry with metal centres and identify structural variations with existing thiosalicylate metal complexes.

Results and discussion

Synthesis of selenosalicylic acid

As shown in Scheme 1, selenosalicylic acid **2** was prepared *via* 2,2′-diselenobisbenzoic acid **3**. First, a solution of disodium diselenide (Na_2Se_2) was prepared by sonication of selenium powder with sodium hydroxymethanesulfinate dihydrate (rongalite) and sodium hydroxide under a nitrogen atmosphere.[53] A solution of 2-carboxybenzenediazonium chloride (freshly prepared from 2-aminobenzoic acid, sodium nitrite and HCl) was added dropwise to the cooled disodium diselenide solution with stirring while not allowing the temperature to exceed 10 °C. Heating to 90 °C for 4 h followed by acidification with HCl precipitated the crude product which was recovered by filtration

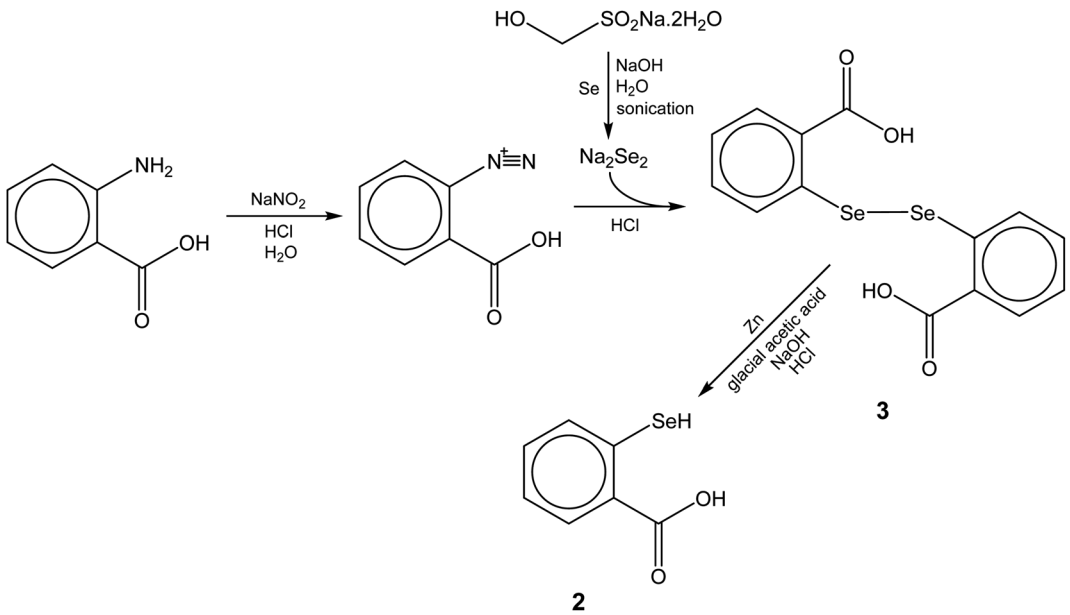

Scheme 1 Synthesis of selenosalicylic acid **2** *via* 2,2′-diselenobisbenzoic acid **3**.

and recrystallised from 1,4-dioxane to give 2,2′-diselenobisbenzoic acid **3** as a beige solid. Selenosalicylic acid **2** was synthesised by adapting the method used for the synthesis of thiosalicylic acid from 2,2′-dithiosalicylic acid[54] by vigorously refluxing **3** in glacial acetic acid with zinc dust for 7 h to give a white slurry. The solid was filtered, suspended in water and a saturated solution of NaOH was added followed by heating to give a light yellow solution containing some residue. This was filtered and the clear filtrate was acidified with concentrated hydrochloric acid to precipitate selenosalicylic acid as a light yellow solid. The product was isolated by filtration, washed with water, and dried under vacuum. It was stored in a tightly sealed vial and (as a precaution against potential air oxidation) used within a few days, and was also characterised by ESI MS, NMR, IR, and elemental analysis.

The negative-ion ESI mass spectrum of selenosalicylic acid showed the expected $[M - H]^-$ ion as the parent peak at *m*/*z* 200.95 with the capillary exit voltage (CEV) varied between 90 and 120 V. At a CEV of 90 V, the peak appearing with the lowest relative intensity (4%) at 156.96 is assigned as a decarboxylated selenosalicylate ion. The spectrum also showed another low intensity peak (10%) that agrees with the deprotonated diselenide, $[(SeC_6H_4CO_2H)_2 - H]^-$, at *m*/*z* 400.89. Upon increasing the CEV to 150 V (Fig. 1), the peak due to decarboxylation became the prominent peak with a 100% intensity relative to the $[M - H]^-$ ion at 96% while the peak of the deprotonated diselenide decreased to 2%. As shown in Fig. 1, the isotope pattern introduced by polyisotopic Se is distinctive compared to the thiosalicylate ligand.

Synthesis of selenosalicylate complexes

Selenosalicylate complexes of nickel, palladium and platinum were prepared in the same way as thiosalicylate complexes reported previously.[55] Reactions of *cis*-$[PtCl_2(PPh_3)_2]$, $[PdCl_2L_2]$ (L or L_2 = PPh_3, dppe, dppf and phen) and $[NiCl_2(dppe)]$ with 1 mole equivalent of selenosalicylic acid **2** in refluxing methanol with added triethylamine base yielded the platinum, palladium, and nickel selenosalicylate complexes, **4a–f** as shown in Scheme 2. These were readily isolated from solution as microcrystalline solids by the addition of water to the cooled reaction mixtures. After drying, the products were purified by redissolving in a small amount of dichloromethane, and crystallising by addition of petroleum spirit. In contrast, the analogous reaction between $[PdCl_2(bipy)]$ (bipy = 2,2′-bipyridine) and **2** did not give the expected chelate as in the above complexes, but instead the suspected dimeric product $[\{Pd(bipy)\}_2(Cl)(SeC_6H_4CO_2)]Cl$ **4g** was isolated.

The synthesis of organo-ruthenium, -rhodium and -iridium complexes followed the above method for the platinum, palladium and nickel complexes, and in conformity to their thiosalicylate analogs.[56] Complexes **4h–k** were prepared by refluxing $[LMCl_2(PPh_3)]$ [M = Ru, L = η^6-*p*-cymene or η^6-C_6Me_6; M = Rh or Ir, L = η^5-C_5Me_5 (Cp*)] with 1 mole equivalent of selenosalicylic acid **2** and triethylamine in methanol. The products were precipitated from the reaction solutions by the addition of water. A solution of the dimeric complex **4l** resulted from a refluxed mixture of $[Cp^*RhCl_2]_2$ and 2 mole equivalents of selenosalicylic acid in methanol with added triethylamine. Microcrystals of the product were obtained after water was added and the mixture allowed to stand for two days.

Finally, the cycloaurated gold(III) complex **4m** was synthesised and isolated as a greenish-yellow solid by room-temperature reaction of benzylpyridylgold(III) chloride with an equivalent amount of selenosalicylic acid in the presence of triethylamine in methanol. The attempted preparation of $[Au(SeC_6H_4CO_2H)(PPh_3)]$ by treating an ethanolic suspension of $[AuCl(PPh_3)]$ with 1 mole equivalent of selenosalicylic acid and one equivalent of NaOH instead resulted in the doubly-aurated **4n** as identified by microelemental analysis, ESI MS and NMR. Cycloaurated gold(III)[1,57–59] and phosphine gold(I)[1,60] complexes containing the thiosalicylate ligand have been reported previously.

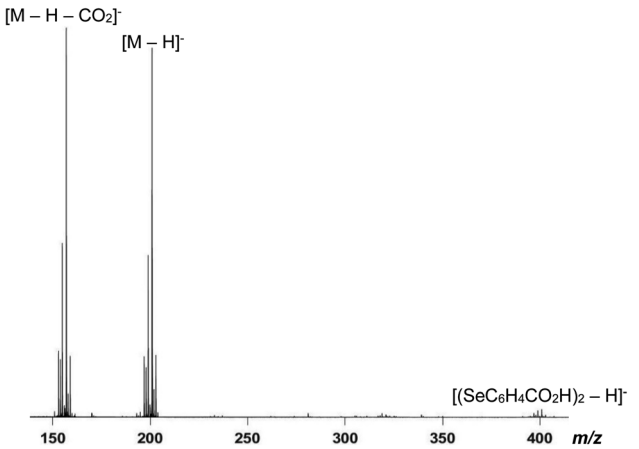

Fig. 1 Negative-ion ESI mass spectrum of selenosalicylic acid **2** at a capillary exit voltage of 150 V, showing the $[M - H]^-$ ion and the decarboxylated fragment ion.

ESI MS characterisation of selenosalicylate complexes

The ESI mass spectrum of **4a** recorded at a capillary exit voltage (CEV) of 60 V showed a low intensity $[M + H]^+$ ion (*m*/*z* 919.86) while the $[M + Na]^+$ peak (*m*/*z* 941.76) is the base peak. Aggregate ions were observed at *m*/*z* 1860.51 for $[2M + Na]^+$ and *m*/*z* 2778.24 for $[3M + Na]^+$. The sodium adducts resulted from the addition of sodium formate in methanol following the observation that the complexes easily picked adventitious Na ion from the instrument. Typical of complexes with a triphenylphosphine ancillary donor, ions formed by loss of PPh_3 were observed at *m*/*z* 1598.51 and 2516.24, assigned to $[2M + Na - PPh_3]^+$ and $[3M + Na - PPh_3]^+$ respectively. At CEV of 240 V, further fragment ions were observed comprising the cyclometallated ion $[Pt(C_6H_4PPh_2)(PPh_3)]^+$[55] at *m*/*z* 717.95 and $[M + Na - PPh_3]^+$ at *m*/*z* 679.76. A fragment from the decarboxylation of the latter ion was observed as $[M + Na - PPh_3 - CO_2]^+$ at *m*/*z* 635.83. Decarboxylation is a common phenomenon for aryl carboxylic acids and has been reported in complexes of thiosalicylic acid,[55,61] possibly occurring by a rearrangement step following the loss of CO_2 to give a carbon-metal bonded

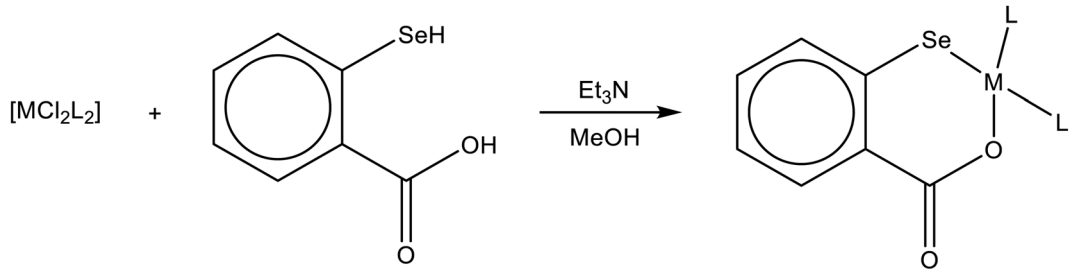

Complex	M	L or L-L
4a	Pt	PPh_3
4b	Pd	PPh_3
4c	Pd	$Ph_2PCH_2CH_2PPh_2$ (dppe)
4d	Pd	1,10-phenanthroline (phen)
4e	Pd	$Fe(C_5H_4PPh_2)_2$ (dppf)
4f	Ni	dppe

Scheme 2 Preparation of platinum, palladium, and nickel selenosalicylate complexes.

fragment.[62] Additional fragment ions were observed due to Se loss when the CEV was increased up to 240 V, with the observation of $[2M + Na - PPh_3 - Se]^+$ and $[M + Na - PPh_3 - CO_2 - Se]^+$ at *m/z* 1518.76 and 556.80 respectively. The σ-bond in C–Se compounds is weaker than the corresponding C–S in analogous sulfur compounds because of the lower electronegativity of selenium,[63] leading to a faster C–Se bond breaking even under mild conditions.

The spectrum of **4b** follows a similar pattern as **4a** with the observation of the $[M + H]^+$ ion at *m/z* 831.09 at a CEV of 60 V. The sodium adduct $[M + Na]^+$ (*m/z* 853.07) formed the most prominent peak at this voltage and appeared with the aggregate ions $[2M + Na]^+$ (*m/z* 1683.06, CEV 60 V) and $[3M + Na]^+$ (*m/z* 2513.63, CEV 60 V). Other observed ion peaks emanating from the fragmentation of these major ones observed at 60 V include $[2M + Na - PPh_3]^+$ (*m/z* 1420.99), $[3M + Na - PPh_3]^+$ (*m/z* 2250.93), $[3M + Na - 2PPh_3]^+$ (*m/z* 1987.89), and $[2M - 2PPh_3]^+$ (*m/z* 1136.52). At higher voltages up to 150 V, more peaks emerged corresponding to $[M + H - PPh_3]^+$ (*m/z* 568.99), $[M + Na - PPh_3]^+$ (*m/z* 590.97), $[M + Na - PPh_3 - Se]^+$ (*m/z* 511.05), $[M + Na - PPh_3 - CO_2]^+$ (*m/z* 546.98), $[2M + Na - PPh_3 - Se]^+$ (*m/z* 1341.07), $[3M + Na - PPh_3 - Se]^+$ (*m/z* 1908.48), $[2M + Na - 3PPh_3]^+$ (*m/z* 896.82), $[2M + H - PPh_3]^+$ (*m/z* 1399.98), $[2M + Na - PPh_3 - Se]^+$ (*m/z* 1341.07), $[2M + H - PPh_3 - Se]^+$ (*m/z* 1319.07), $[3M + Na - 3PPh_3]^+$ (*m/z* 1725.80), and $[2M + Na - 2PPh_3]^+$ (*m/z* 1158.89). The calculated and experimental isotope patterns of the peaks match perfectly as exemplified by that of $[M + H]^+$ in Fig. 2.

The spectra of the diphosphine complexes **4c**, **4d**, **4e** and **4f** showed ions and fragmentation similar to **4a** and **4b** while **4g** showed a parent peak at *m/z* 760.68 which agrees with the ion $[\{Pd(bipy)\}_2(Cl)(SeC_6H_4CO_2)]^+$ where the selenosalicylate Se is suspected to bridge two palladium metal centres as in known thiosalicylate complexes.[1,64] A similar M^+ ion, $[\{Pd(dppe)\}_2(Cl)(SeC_6H_4CO_2)]^+$ was observed as an additional low intensity peak in **4c** at *m/z* 1244.71.

The ruthenium, rhodium, and iridium complexes **4h–k** share the same features as the platinum, palladium, and nickel complexes in terms of fragmentation due to loss of PPh_3, CO_2, and Se, and in aggregate ion formation. For example, the positive-ion spectrum of $[Cp^*Rh(SeC_6H_4CO_2)(PPh_3)]$ **4j**, obtained at a CEV of 60 V, shows a very low intensity $[M + H]^+$ peak at *m/z* 700.91 (3%) and the sodium adduct $[M + Na]^+$ (*m/z* 722.90) at 80% relative intensity. The $[2M + H]^+$ aggregate ion is seen at *m/z* 1400.82 while the most prominent peak with 100% relative intensity corresponds to the $[2M + Na]^+$ ion (*m/z* 1422.81). The $[3M + Na]^+$ ion (*m/z* 2120.70) and fragment ions such as $[3M + Na - PPh_3]^+$ (*m/z* 1858.66), $[3M + Na - 2PPh_3]^+$ (*m/z* 1596.63), $[2M + Na - PPh_3 - Se]^+$ (*m/z* 1081.24), $[2M + Na - PPh_3 - 2Se]^+$ (*m/z* 1000.92), and $[2M + Na - 2PPh_3]^+$ (*m/z* 898.73) were also observed. Upon varying the CEV between 90 and 150 V, additional fragment ions emerged for $[2M + Na - PPh_3]^+$ (*m/z* 1160.78), $[M + Na - PPh_3]^+$ (*m/z* 460.86), and $[M + Na - PPh_3 - CO_2]^+$ (*m/z* 416.89). Similar behaviour was observed in the spectra of **4j**, **4k**, **4h**, and **4i**. Even at low voltage, the dimer **4l** undergoes fragmentation to give the monomer whose sodium adduct was observed as $[M + Na - Cp^*RhSeC_6H_4CO_2]^+$ at *m/z* 460.36, an occurrence also found in $[2M + Na - Cp^*RhSeC_6H_4CO_2]^+$ (*m/z* 1334.55). The former ion was present at much higher relative intensity (up to 61%) when the CEV was

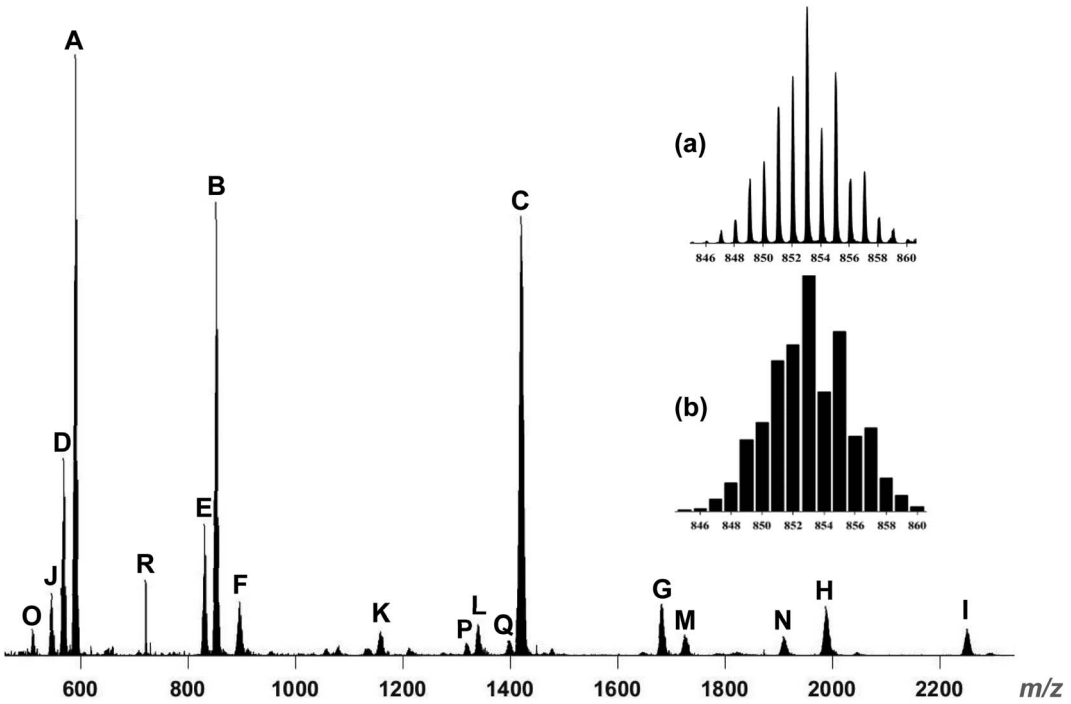

Fig. 2 Positive-ion ESI mass spectrum of $[Pd(SeC_6H_4CO_2)(PPh_3)_2]$ **4b** at 150 V showing the formation of aggregate and fragment ions. Insets (a) and (b) are the experimental and calculated isotope patterns of the $[M + Na]^+$ ion, B. Legend: A = $[M + Na - PPh_3]^+$ (*m*/*z* 590.97); B = $[M + Na]^+$ (*m*/*z* 853.07); C = $[2M + Na - PPh_3]^+$ (*m*/*z* 1420.99); D = $[M + H - PPh_3]^+$ (*m*/*z* 568.99); E = $[M + H]^+$ (*m*/*z* 831.09); F = $[2M + Na - 3PPh_3]^+$ (*m*/*z* 896.82); G = $[2M + Na]^+$ (*m*/*z* 1683.06); H = $[3M + Na - 2PPh_3]^+$ (*m*/*z* 1987.89), I = $[3M + Na - PPh_3]^+$ (*m*/*z* 2250.93), J = $[M + Na - PPh_3 - CO_2]^+$ (*m*/*z* 546.98); K = $[2M + Na - 2PPh_3]^+$ (*m*/*z* 1158.89); L = $[2M + Na - PPh_3 - Se]^+$ (*m*/*z* 1341.07); M = $[3M + Na - 3PPh_3]^+$ (*m*/*z* 1725.80); N = $[3M + Na - PPh_3 - Se]^+$ (*m*/*z* 1908.48); O = $[M + Na - PPh_3 - Se]^+$ (*m*/*z* 511.05); P = $[2M + H - PPh_3 - Se]^+$ (*m*/*z* 1319.07); Q = $[2M + H - PPh_3]^+$ (*m*/*z* 1399.98); R = $(PPh_3)_2Au^+$ from adventitious Au(I) in the instrument and the lost PPh_3 ligand.

increased to 210 V and occurred among other fragments including $[M + H - Cp^*RhSeC_6H_4CO_2]^+$ (*m*/*z* 438.86) and $[M + H - Cp^*RhSeC_6H_4CO_2 - CO_2]^+$ (*m*/*z* 416.85).

The gold(III) complex **4m** displayed a series of sodiated aggregate ions $[M + Na]^+$, $[2M + Na]^+$, $[3M + Na]^+$ and $[4M + Na]^+$. The spectrum of the product of the reaction of $[AuCl(PPh_3)]$ with selenosalicylic acid **2** was expected to yield $[Au(SeC_6H_4CO_2H)(PPh_3)]$ analogous to the known $[Au(SC_6H_4CO_2H)(PPh_3)]$,[60] but instead gave the neutral zwitterionic complex $[(PPh_3Au)_2SeC_6H_4COO]$ **4n**. One of the peaks observed in the spectrum agreed with the triply aurated selenosalicylate complex $[\{(PPh_3)Au_2SeC_6H_4C(O)OAu(PPh_3)\}]^+$ which can alternatively be written as $[M + Au(PPh_3)]^+$, designated as **4n′**, and involving three metal centres. It is proposed that two of these are bound to the Se donor of one selenosalicylate ligand while the third is coordinated to the carboxylate-O atom. This form of coordination of Au(I) has been reported previously for mercaptoacetate and mercatopropionate ligands.[65]

NMR spectroscopic characterisation

The proton NMR spectrum of selenosalicylic acid **2** in d_6-DMSO shows a singlet at δ 5.75, tentatively assigned to the selenol (–SeH) proton in keeping with the appearance of the related thiosalicylate (–SH) proton within this region.[66] The OH proton of the carboxylic acid group is not observed. With the presence of a broad signal at δ 3.45 assigned to HOD, the –OH proton is likely to have undergone an exchange. The aromatic proton signals are distinctive, with the H-6 signal appearing as a doublet of doublets at δ 8.03, and H-3 showing with the same multiplicity at δ 7.67. The triplet of doublet signals at δ 7.48 and 7.35 are assigned as H-4 and H-5 respectively. The $^{13}C\{^1H\}$ NMR spectrum of the compound clearly showed a signal at δ 169.10, typical of a carboxylic C=O. The other six signals between δ 134.03 and 127.00 are in agreement with aromatic carbons.

The absence of the selenol proton signal in the ^1H NMR spectra of all complexes is an indication of a bound selenolate group. For $[Pt(SeC_6H_4CO_2)(PPh_3)_2]$ **4a**, signals from the aromatic protons of the ligand and the two triphenylphosphines appear between δ 7.74 and 7.02. The spectra of the other phosphine complexes **4b**, **4c**, **4e** and **4f** also follow this pattern. In the case of the palladium and nickel complexes **4c** and **4f**, the chemical shifts of the dppe auxiliary ligand are observed as two separate multiplets of two CH_2 protons each, at δ 2.23 and 2.51, and δ 2.02 and 2.36 respectively. Similarly, the ferrocene protons of the dppf auxiliary ligand in **4e** are seen as four singlets between δ 4.76 and 3.76. The combination of the phenanthroline or bipyridine and selenosalicylate protons are observed between δ 7.14 and 9.32, and δ 7.11 and 9.12 in **4d** and **4g** respectively.

The $^{31}P\{^1H\}$ NMR spectroscopic properties of **4a–c** and **4e–4f** are consistent with their formulation as selenosalicylate complexes. For **4a**, the different *trans* influences of the selenium

and oxygen donor atoms are reflected in different $^{1}J_{Pt-P}$ values for the two phosphorus atoms. Thus, the two resonances at δ 21.5 and 7.2 with $^{1}J_{Pt-P}$ couplings of 2897 and 3917 Hz are assigned as PPh_3 ligands *trans* to Se and O respectively. In comparison, the coupling constant of PPh_3 *trans* O in the thiosalicylate analog $[Pt(SC_6H_4CO_2)(PPh_3)_2]$ is 3899 Hz while PPh_3 *trans* S is 2884 Hz.[55] *trans*- and *cis*-$^{2}J_{P-Se}$ coupling is also observed, for example in **4a** where the coupling constants are 49 Hz (*trans*) and 27 Hz (*cis*). This is attributed to the NMR-active ^{77}Se isotope ($I = \frac{1}{2}$, natural abundance 7.6%).[67] The $^{31}P\{^{1}H\}$ NMR spectrum of **4f** showed satellite peaks due to ^{77}Se coupling, however, it is unclear how the $^{2}J_{P-Se}$ coupling constants for the phosphines *trans* and *cis* to the selenium donor atom seem to have similar values in the Ni(II) complex. The palladium complex **4b** has two AB pattern doublets at δ 32.9 and 18.4, having $^{2}J_{P-P}$ 30 Hz, but the satellite peaks due to $^{2}J_{P-Se}$ coupling are not visible due to overlapping main signals.

The ^{1}H NMR spectra of the pentamethylcyclopentadienyl complexes $[Cp^*Rh(SeC_6H_4CO_2)(PPh_3)]$ **4j** and $[Cp^*Ir(SeC_6H_4CO_2)(PPh_3)]$ **4k** indicate slight variations in chemical shifts since the complexes only differ by the metal ions. Proton signals of the aromatic groups of the selenosalicylate ligand and the triphenylphosphine auxiliary ligand appeared from δ 6.92–7.88 and 6.90–7.88 for Rh and Ir respectively. The rhodium complex showed a singlet for the methyl groups of the Cp* ligand at δ 1.27 while in the iridium complex, this appeared at δ 1.28. The aromatic region in the spectrum of $[(p\text{-cym})Ru(SeC_6H_4CO_2)(PPh_3)]$ **4h** is closely related to these, only differing in the four aromatic protons of *p*-cymene, seen as four doublets between δ 4.45 and 5.36, while the doublet resonances due to the *p*-cymene isopropyl methyl protons were observed at δ 1.18 and 1.07, and a heptet for $-CHMe_2$ at δ 2.45. The remaining methyl protons *para* to the isopropyl substituents in *p*-cymene are seen at δ 1.97. The inequivalence of the aromatic protons and isopropyl methyl protons of the *p*-cymene group is attributed to the unsymmetrical ruthenium centre in the complex.[68] For the related hexamethylbenzene complex **4i**, the singlet occurring at δ 1.70 is assigned to the $18C_6Me_6$ protons. The $^{31}P\{^{1}H\}$ NMR of this set of complexes displayed the expected singlet resonances for the triphenylphosphine ligand in the ruthenium and iridium complexes at δ 35.5, 29.4 and 7.5 for **4h**, **4i** and **4k** respectively. However, for the rhodium complex **4j**, the resonance is seen as a doublet at δ 34.0 due to $^{1}J_{Rh-P}$ coupling of 150 Hz. Unlike in most of the Pt, Pd and Ni complexes, satellite peaks from $^{2}J_{P-Se}$ coupling were not visible in the octahedral Ru, Rh, and Ir complexes.

The ^{1}H NMR spectrum of the dimeric complex $[\{Cp^*Rh(SeC_6H_4CO_2)\}_2]$ **4l** showed the aromatic protons of the selenosalicylate ligand between δ 7.18 and 8.21 along with the singlet of the Cp* methyl protons at δ 1.34. The complex equally gave an excellent $^{13}C\{^{1}H\}$ NMR spectrum with the carboxylate-C of the selenosalicylate ligand observed at δ 171.00. The signals between δ 126.65 and 139.95 were assigned to the aromatic carbons of the ligand while the doublet at δ 94.99 and the singlet at δ 8.68 are due to the ring carbon and CH_3 of Cp* respectively.

The gold(III) complex $[(bp)Au(SeC_6H_4CO_2)]$ **4m** (bp = cycloaurated benzylpyridyl ligand) displayed a ^{1}H NMR spectrum with aromatic protons between δ 7.09 and δ 9.16, and a signal at δ 4.30 assigned as the $-CH_2-$ linkage. The $^{13}C\{^{1}H\}$ NMR showed a peak at δ 170.13 for the carboxylate-C and δ 47.66 for the $-CH_2-$ while those from δ 154.83 to 124.61 are of the phenyl and pyridyl rings. The structure was predicted based on the reported isomer of thiosalicylate analogues[57–59] where the C and S donor ligands are mutually *cis* based on the antisymbiosis rule.[69]

The ^{1}H NMR of the gold(I) complex **4n** in d_6-DMSO gave signals between δ 7.02 and 7.92, attributed to the aromatic protons of the selenosalicylate ligand and triphenylphosphine. In the $^{31}P\{^{1}H\}$ NMR spectrum, the prominent singlet at δ 35.6 is assigned to the two chemically equivalent phosphorus atoms of the $Se\{Au(PPh_3)\}_2$ moiety. An associated low-intensity signal at δ 25.6 is tentatively assigned as the phosphorus atom of the $(Ph_3P)Au-O$ unit of the triply aurated complex **4n′**. These values are close to those reported for the corresponding mercaptoacetate and mercaptopropionate complexes of Au(I) where the $(Ph_3P)Au-O$ and $S\{Au(PPh_3)\}_2$ signals were recorded as δ 27.0 and 34.1, and δ 27.3 and 34.3 respectively.[65]

IR characterisation of selenosalicylic acid 2 and selenosalicylate complexes

Selenosalicylic acid shows a stretching vibration due to the uncoordinated –SeH at 2562 cm^{-1} similar to that of the thiol (–SH) occurring within this range,[70,71] and a broad band at 3437 cm^{-1} from the –OH of the carboxylic acid group. A very strong band due to the carboxylic C=O was observed at 1672 cm^{-1} while the C–O stretch of this group was identified as a strong band at 1265 cm^{-1}. Other strong signals include the vibration at 1027 cm^{-1} interpreted as the C–H in-plane bending mode of the ligand's aromatic ring, and the C–Se stretch from the 1,2-disubstituted aromatic ring at 738 cm^{-1}, assigned by comparison with thiosalicylate.[55]

In the complex $[Pt(SeC_6H_4CO_2)(PPh_3)_2]$ **4a** the disappearance of the –SeH and –OH bands are indications of coordination of the deprotonated groups, as the C=O vibration shifts to 1621 cm^{-1}.

X-ray crystal structures of selected selenosalicylate complexes

X-ray structure determinations have been carried out on a selection of selenosalicylate complexes, confirming their identities. The structure of the Pt complex **4a** is shown in Fig. 3, together with the atom numbering scheme, while selected bond lengths and angles are given in Table 1. The selenosalicylate ligand of **4a** is disordered with the positions of the selenium and the carbon and oxygen atoms of the carboxylate group, each occupying two sites, and was modelled with occupancies of 90 and 10%. The carbon atom and one oxygen atom of the carboxylate group of the minor orientation, C7B and O2B, were refined with isotropic thermal displacement.

The structure consists of the expected square-planar metal–ligand coordination geometry of the $PtSeOP_2$ core where the metal is chelated by Se and O donor atoms of the selenosalicylate ligand and bonded to the two phosphorus atoms. The Pt

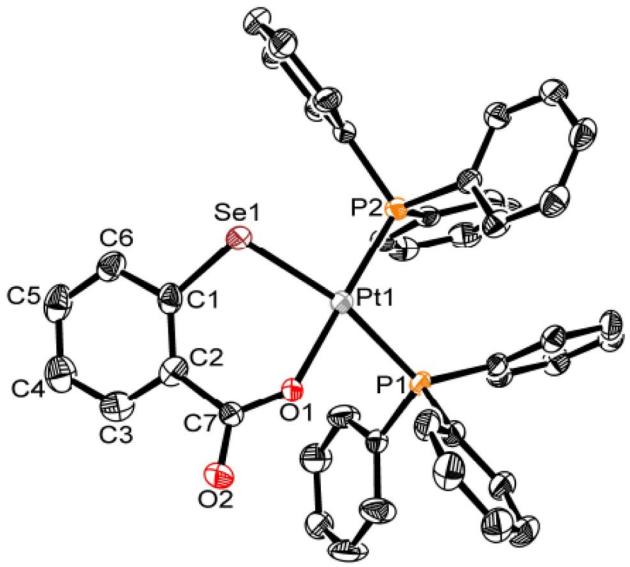

Fig. 3 Molecular structure and numbering scheme of [Pt($SeC_6H_4CO_2$)(PPh_3)$_2$] **4a**. Hydrogen atoms and disorder in ligand are omitted for clarity. Thermal ellipsoids are at 50% probability.

Table 1 Selected bond lengths (Å) and angles (°) of [Pt($SeC_6H_4CO_2$)(PPh_3)$_2$] **4a**

Pt1–Se1	2.4301(4)	C1–C2	1.407(5)
Pt1–O1	2.051(5)	C2–C3	1.402(5)
Pt1–P1	2.3035(7)	C3–C4	1.375(5)
Pt1–P2	2.2367(7)	C4–C5	1.384(5)
O1–C7	1.286(5)	C5–C6	1.390(4)
Se1–C1	1.892(3)	C6–C1	1.402(4)
O2–C7	1.235(5)	C7–C2	1.500(5)
P1–Pt1–P2	100.11(3)	P1–Pt1–Se1	166.96(2)
P2–Pt1–O1	177.32(16)	Se1–Pt1–O1	88.08(14)
P1–Pt1–O1	79.88(14)	P2–Pt1–Se1	92.15(2)
Pt–Se1–C1	101.27(10)	Pt1–O1–C7	135.6(5)
O1–C7–O2	119.9(5)	O1–C7–C2	121.2(5)
O2–C7–C2	118.8(4)	C7–C2–C3	115.0(3)
C2–C3–C4	121.9(3)	C3–C4–C5	119.7(4)
C4–C5–C6	120.0(3)	C5–C6–C1	121.4(3)
C6–C1–C2	119.2(3)	C7–C2–C1	126.9(3)
C2–C1–Se1	126.3(2)	C6–C1–Se	114.5(3)

atom is 0.018 Å below the plane defined by the Se, O and two P donors, with the plane having a r.m.s. deviation of 0.066 Å. The dihedral angle between the plane of the $PtSeOP_2$ coordination sphere and that of the C1–C6 ring is 137°. While the plane defined by the selenosalicylate ring and the Se1 and C7 atoms is nearly coplanar with a r.m.s. deviation of 0.012 Å, the inclusion of O1 and O2 in the plane reveals the displacement of these atoms by 0.301 and 0.331 Å above and below the plane respectively, because of the twisting of the C2–C7 bond. The deviation of the coordination sphere of **4a** from perfect planarity [as evident in the bond angles P1–Pt1–P2 100.11(3)° and Se1–Pt–O1 88.08(14)°] reflects the steric interactions of the bulky triphenylphosphine ligands and the natural bite of the selenosalicylate ligand. The former angle is quite similar to the one reported for the thiosalicylate analogue [Pt($SC_6H_4CO_2$)(PPh_3)$_2$] (100.5°),[55] but the latter varies by 3.38°. As in the thiosalicylate complex, the Pt1–P1 bond distance (P *trans* Se) of **4a** [2.3035(7) Å] is slightly longer than Pt1–P2 (P *trans* O) [2.2367(7) Å], consistent with a higher *trans*-influence of Se relative to O.

The Pt1–Se1 distance of 2.4301(4) Å is, as expected, slightly longer than the Pt–S bond distance [2.322(2) Å] in the thiosalicylate complex [Pt($SC_6H_4CO_2$)(PPh_3)$_2$].[55] Similarly, the Pt1–Se1–C1 bond angle of 101.27(10)° in **4a** is slightly more acute than in the thiosalicylate analogue [Pt($SC_6H_4CO_2$)(PPh_3)$_2$] [103.7(2)°], while the Pt1–O1–C7 angle of 135.6(5)° and the Se1···O1 bite distance of 3.127 Å (135.8° and 2.99 Å in the thiolate) are quite similar.

Attempts at growing single crystals of **4h** resulted in deposition of single crystals of the dimeric complex [{(*p*-cym)Ru($SeC_6H_4CO_2$)}$_2$] **4h′**. X-ray diffraction studies of this and the dinuclear rhodium complex **4l**, as well as the mononuclear phosphine complex **4k** were carried out. The structure of **4h′** indicates the loss of the triphenylphosphine ligand and subsequent dimerisation of the fragment. The molecular structures of the complexes are shown in Fig. 4–6.

In the ruthenium and rhodium dimers (**4h′** and **4l**) the metal centres have the distorted octahedral, 'piano-stool' coordination geometry characteristic of such complexes. The asymmetric unit of the two complexes is half a molecule of the dimer. Each metal is bound to the selenolate and carboxylate groups of the selenosalicylate to form a six-membered ring while the M–Se′ bond to the second selenosalicylate ligand forms the third leg of the 'stool' and the π hydrocarbon constitutes the 'seat'. The dimer is formed by the bridging of the selenolates to the other metal centre to give a M–Se–M–Se four-membered core. As in the platinum complex, the metal-selenosalicylate ring system in **4h′** is folded, predominantly at the ruthenium and the carboxylate as evident in the Ru1–O1–C7 obtuse angle of 135.7(2)° with the carboxylate twisted by 42.21° from the selenosalicylate phenyl ring. These values are smaller in the Rh complex **4l**, where the obtuse angle of 134.89(18)° and carboxylate twist of

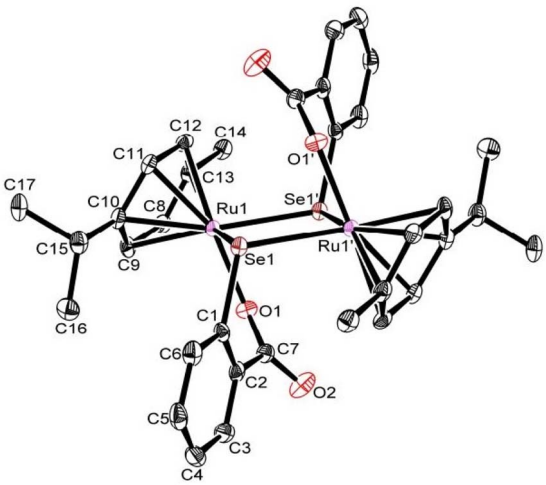

Fig. 4 Molecular structure and numbering scheme of [{(*p*-cym)Ru($SeC_6H_4CO_2$)}$_2$] **4h′**. Hydrogen atoms are omitted for clarity. Thermal ellipsoids are at 50% probability.

35° are found. The Ru–Se bond length of 2.5139(4) Å in **4h′** is similar to that of Ru–Se′ [2.4862(4) Å] but slightly longer than the Ru–S and Ru–S′ bonds [2.3848(4) and 2.4177(4) Å] in the analogous thiosalicylate complex [{(*p*-cym)Ru($SC_6H_4CO_2$)}$_2$][56] and similar to the Rh–Se and Rh–Se′ bond distances [2.5060(3) and 2.4617(3) Å] of **4l**. Similarly, the Ru–S–Ru′ angle of 99.286(15)° in [{(*p*-cym)Ru($SC_6H_4CO_2$)}$_2$] is only 1° larger than the Ru1–Se1–Ru1′ bond angle of 98.23(10)°. This, however, is smaller in the Rh complex, being 95.56(10)°. The Se1–M–Se1′ bond angle in the Rh complex **4l** is larger than in the Ru complex **4h′** [84.88(10) *versus* 81.77(10)°], a trend also observed in the thiosalicylate complex although the angles vary considerably in the two ligand systems. Equivalent O1–M–Se1 acute angles [**4h′** 87.79(6) and **4l** 88.71°] are substantially larger than the pair of O1–M–Se1′ [**4h′** 76.48(6) and **4l** 75.76(5)°] with about the same difference between O–M–S and O–M–S′ of the thiosalicylate. The M−O distances in the ruthenium and rhodium complexes **4h′** and **4l** are identical [Ru–O 2.099(2) and Rh–O 2.1000(18) Å]. However, the molecular geometries of the complexes vary significantly in the inclination angle of the selenosalicylate phenyl ring relative to the π-hydrocarbon ligand plane. While the angle is 11.08° in the rhodium complex **4l**, it is 22.52° in the ruthenium complex **4h′**, both being smaller by 1° than the equivalents in the thiosalicylate complexes. The disparity likely stems from the effects of steric interactions between the selenosalicylate and π-hydrocarbon ligands although the Cp* or *p*-cymene and selenosalicylate units are far apart and intramolecular atomic contacts are quite long [closest contacts: Ru complex 3.538(5) Å for C1–C12 and Rh complex 3.415(4) Å for C1–C16]. As *p*-cymene has only two substituents [–CH_3 and –$CH(CH_3)_2$] in *para*-positions, less steric interaction is expected in the ruthenium complex since the selenosalicylate could fit into a pocket of reduced steric interaction compared to the rhodium complex with a fully substituted Cp*. The non-equidistant Ru–C bonding between Ru and *p*-cymene in the ruthenium complex [from Ru1–C12 2.161(3) Å to Ru1–C13 2.252(3) Å] might equally be related to the steric interaction of the partially substituted *p*-cymene and the selenolate ligand. Stronger interactions by the fully substituted Cp* could be responsible for the larger Se1–M–Se1′ bond angle in **4l** compared to **4h′**.

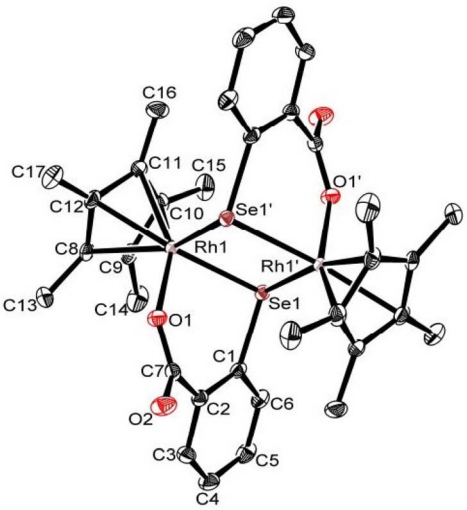

Fig. 5 Molecular structure and numbering scheme of [{Cp*Rh($SeC_6H_4CO_2$)}$_2$].[41] Hydrogen atoms are omitted for clarity. Thermal ellipsoids are at 50% probability.

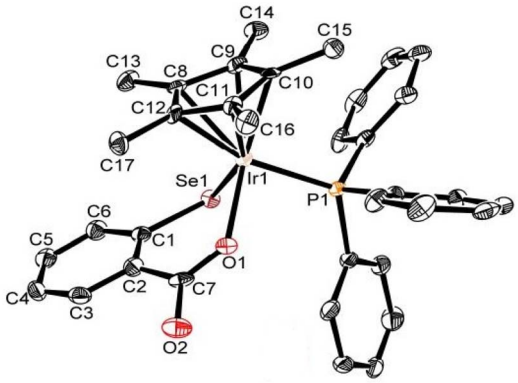

Fig. 6 Molecular structure of the non-disordered molecule of **4k** showing the numbering scheme. The water molecule and hydrogen atoms are omitted for clarity. Thermal ellipsoids are at 50% probability.

The iridium phosphine complex **4k** (Fig. 6) crystallises with two molecules of the compound and one molecule of water in the asymmetric unit. The selenosalicylate ligand of one of the molecules of **4k** is disordered with the positions of the selenium and atoms of the carboxylate group, each occupying two sites, and was modelled with occupancies of 65 and 35%. One oxygen atom of the ligand of the minor orientation, O2C, is virtually coincident with the selenium atom of the major orientation, Se1B, necessitating its refinement with isotropic thermal displacement. Akin to the Ru and Rh complexes, the Ir centre is coordinated to the deprotonated selenosalicylate at the Se and carboxylate-O atoms to form a six-membered chelate system while the Ir–P bond constitutes the third leg of the 'piano-stool'. The selenosalicylate ligand is more folded than in the dimers (**4h′** and **4l**) with the carboxylate twisting in Ir1–O1–C7, and the Ir1–Se1–C1 angle being smaller [131.3(3) and 98.12(14)° respectively], as in the slightly smaller O1–Ir1–Se1 angle [86.05(9)°]. However, the Ir1–Se1 and Ir1–O1 bonds have similar distances [2.4733(5) and 2.110(3) Å] with the corresponding ones in the dimers. The water molecule exhibits an intermolecular hydrogen interaction with the unbonded carbonyl oxygen atom. The chiral iridium centre in **4k** is *pseudo*-tetrahedrally coordinated by four groups: Cp*, PPh_3, the deprotonated selenol and the deprotonated carboxylate. Thus, the unit cell reflects two enantiomers where there are two molecules of each enantiomer.

Hirshfeld surface analysis of selected complexes

Hirshfeld surface (HS) analysis was carried out to quantify and visualise the various intermolecular interactions[72] in the crystal structures of **4h′** and **4k** by mapping the direction and strengths of the contacts within the crystals onto Hirshfeld surfaces using the descriptor d_{norm}. The normalised contact distance (d_{norm}) is

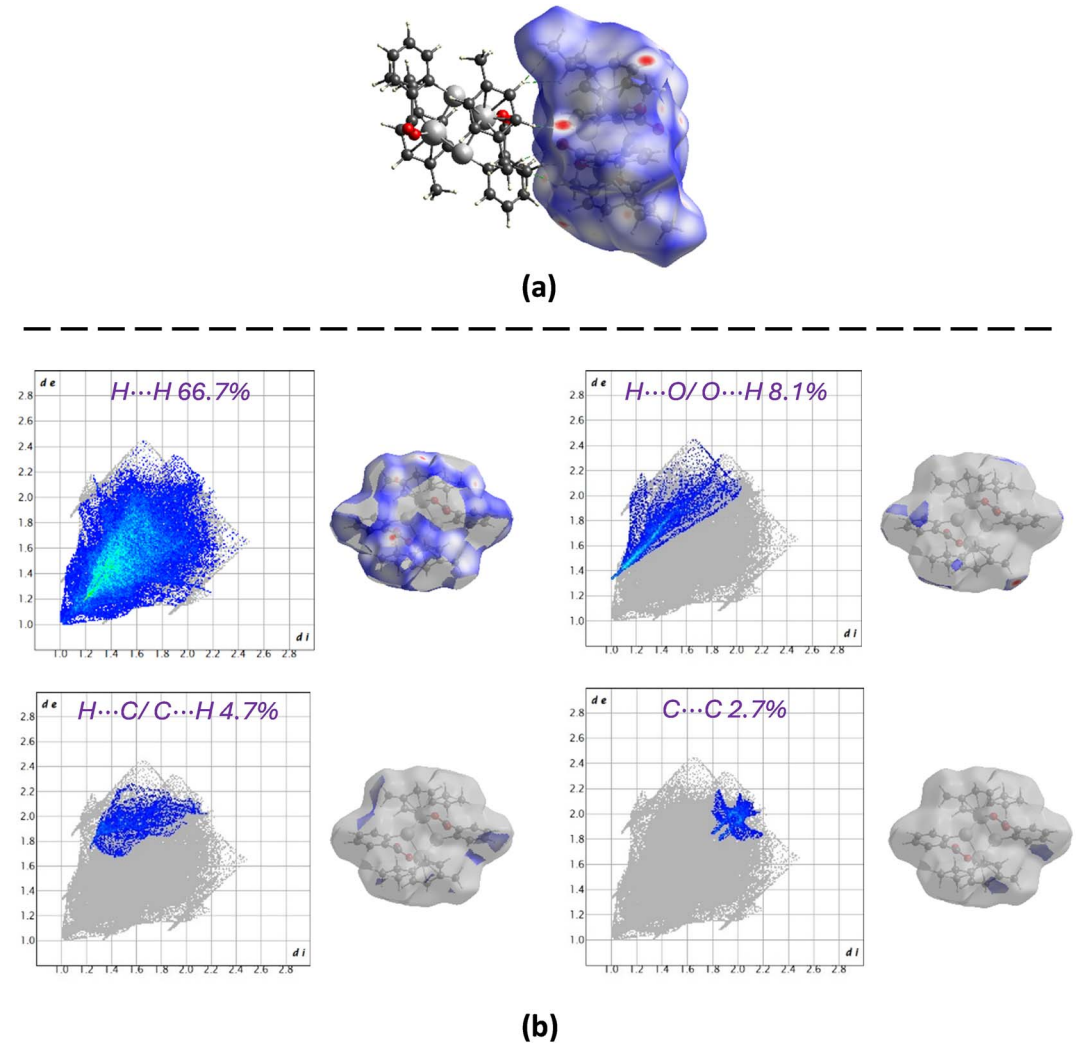

Fig. 7 (a) Intermolecular interactions on Hirshfeld surface and (b) 2D fingerprint plots in **4h′**.

based on the distances between nearest atoms present inside (d_i) and outside (d_e) the surface.[73] Fig. 7a shows the visualisation of the Hirshfeld three-dimensional d_{norm} surface mapped on the asymmetric unit of **4h′**. In **4h′**, the relatively intense red spots on the surface are located on the free carbonyl oxygen atom of the selenosalicylate ligand and methyl hydrogen atom of a close *p*-cymene moiety and indicate C–H···O interactions whereas the different shades of light-red spots constitute weaker C–H···H–C contacts of the isopropyl hydrogen and the *p*-cymene ring hydrogen of another molecule, and the C–H···O contacts of the bonded carbonyl O-atom and an isopropyl hydrogen. The C–H···O interactions in **4k** emanate from the ring C–H and carbonyl oxygen of two ligand groups while the light red spots are attributed to interactions between $-CH_3$ of Cp* or –phenyl ring of PPh_3 and ligand –C=O. The two-dimensional fingerprint plots of **4h′** (Fig. 7b) show the intermolecular contacts and their percentage distribution on the Hirshfeld surface. Globally, the crystal packing is dominated by H···H contacts at 66.7%, as widely scattered points of high density because of the large hydrogen content of the molecule, with the tip at $d_e = d_i \approx 1.0$ Å. The H···O/O···H interactions constitute only 8.1% of the contacts. Small contributions from other interatomic contacts include C···H/H···C (4.7%), C···C (2.7%), and Se···H/H···Se (1.3%). In **4k**, the H···H contacts constitute 64.0% while H···O/O···H and C···H/H···C are 6.2 and 9.2% respectively. The large number of H···H contact is suggestive of crystal packing stabilised by van der Waals interactions.[74]

Conclusions

Selenosalicylate complexes of transition metals analogous to previously reported thiosalicylate complexes have been synthesised and characterised for the first time. Selenosalicylic acid was obtained from the reduction of 2,2′-diselenobisbenzoic acid, synthesised by reacting freshly prepared solutions of 2-carboxybenzenediazonium chloride and disodium diselenide. X-ray crystallographic studies and data from other spectroscopic techniques revealed the formation of six-membered chelate rings in all the complexes except in Au(I). The

$[Pt(SeC_6H_4CO_2)(PPh_3)_2]$ complex was found to structurally resemble its thiosalicylate analogue due to the coordination mode and similarities in some bond lengths and angles. However, the Se–Pt–O bite angle and C–O bonds of the carboxylate group significantly vary from the equivalent ones in the thiosalicylate complex. The Ru, Rh and Ir complexes also exhibited the formation of monomeric and dimeric complexes previously reported for thiosalicylate. Similarly, the type of Se-bifurcated doubly aurated complex found in Au(I) is also well known in analogous thiolate chemistry. Hirshfeld surface analysis revealed that H···H contacts are more than other forms of intermolecular interactions in the crystals. ESI MS data of most of the complexes showed the ease of decarboxylation of the ligand both in the free and coordinated state, and the cleavage of the C–Se bond in selenium atom loss.

Experimental

Materials

Rongalite (hydroxymethanesulfinic acid monosodium salt dihydrate), sodium nitrite, 2-aminobenzoic acid, triethylamine, zinc dust and glacial acetic acid were supplied by Sigma-Aldrich while selenium powder was obtained from Ajax Chemicals. The complexes *cis*-$[PtCl_2(PPh_3)_2]$, $[PdCl_2(PPh_3)_2]$, $[PdCl_2(dppf)]$ and $[PdCl_2(dppe)]$ were prepared by addition of the stoichiometric amount of phosphine to a solution of $[MCl_2(cod)]$ (cod = 1,5-cyclo-octadiene, M = Pd,[75] M = Pt[76]) in CH_2Cl_2, followed by precipitation of the product with petroleum spirits.[77] The complexes $[PdCl_2(bipy)]$,[78] $[PdCl_2(phen)]$,[79] $[NiCl_2(dppe)]$,[80] $[(\eta^6\text{-}C_6Me_6)RuCl_2(PPh_3)]$,[81] $[\{(\eta^5\text{-}Cp^*)RhCl_2\}_2]$,[82] $[(\eta^5\text{-}Cp^*)RhCl_2(\text{-}PPh_3)]$[81] and $[(\eta^5\text{-}Cp^*)IrCl_2(PPh_3)]$[83] were prepared by the literature procedures. $[(\eta^6\text{-}p\text{-cym})RuCl_2(PPh_3)]$ was prepared by a slightly modified literature procedure, using ethanol in place of hexane.[84] $[(bp)AuCl_2]$ (bp = 2-benzylpyridyl)[85] and $AuCl(PPh_3)$[86] were prepared by modifications of literature methods, by reaction of $[Me_4N][AuCl_4]$ with 2-benzylpyridine or triphenylphosphine respectively.

Instrumentation

Unless otherwise stated, NMR spectra were recorded in $CDCl_3$ on a Bruker Avance(III) instrument (^{1}H 400 MHz, ^{31}P 162 MHz, ^{13}C 100.6 MHz); coupling constants are in Hz. Microanalytical data were obtained through the Campbell Microanalytical Laboratory, University of Otago, New Zealand. FTIR data were recorded as KBr disks on a PerkinElmer Spectrum 100 instrument in the range 400–4000 cm^{-1}. Melting points were recorded using a Reichert-Jung Thermovar instrument with solid samples.

Synthesis of 2,2′-diselenobisbenzoic acid 3

This was prepared according to a literature method.[53] A two-necked 500 mL round-bottomed flask under nitrogen was charged with hydroxymethanesulfinic acid monosodium salt dihydrate (rongalite, 4.4 g, 28.6 mmol), sodium hydroxide pellets (2.2 g, 55.0 mmol), water (30 mL), and selenium powder (4.4 g, 55.7 mmol), and allowed to sonicate (using a commercial ultrasonic cleaning bath) for 2 h to give a dark-red solution of disodium diselenide (Na_2Se_2).

A solution of sodium nitrite (4.5 g, 65.2 mmol) in water (10 mL) was added dropwise to a stirred solution containing 2-aminobenzoic acid (7.0 g, 51.0 mmol) and concentrated hydrochloric acid (10 mL) in 10 mL of water, maintained at 5–10 °C with an ice bath, to give a solution of 2-carboxybenzenediazonium chloride. The freshly prepared 2-carboxybenzenediazonium chloride solution was then added dropwise, under nitrogen, to the disodium diselenide solution while stirring and maintaining the temperature below 10 °C. After complete addition, the mixture was allowed to reach room temperature and then heated to 90 °C for 4 h, after the N_2 gas evolution had ceased. The reaction mixture was acidified with hydrochloric acid until precipitates stopped forming. The crude solid was collected by filtration and dried under vacuum, and then recrystallised from dioxane to give beige coloured solids of 2,2′-diselenobisbenzoic acid **3**. Yield 7.4 g (72%). ^{1}H and ^{13}C NMR signals resemble those of selenosalicylic acid below except for the absence of an SeH signal. ESI MS: Calculated *m*/*z* 400.88; experimental *m*/*z* 400.87 $[M - H]^-$.

Synthesis of selenosalicylic acid 2

Zinc dust (0.5 g, 76.5 mmol) was added to a mixture containing 2,2′-diselenobisbenzoic acid (1.0 g, 2.5 mmol) and glacial acetic acid (15 mL), and refluxed vigorously for 7 h to give a white slurry. The slurry was filtered to obtain a cake residue which was suspended in water (30 mL) followed by the addition of a 33% solution of NaOH (5 mL). The mixture was then heated for another 20 min., resulting in a light yellow solution containing some residues. This was filtered and the filtrate was acidified with concentrated HCl to precipitate selenosalicylic acid as a light yellow solid. The product was filtered, washed with water (15 mL), dried under vacuum, and stored in a sealed glass vial. Yield (0.5 g, 50%). M.p. >180 °C (decomp.). Found (%): C 42.65, H 2.51; $C_7H_6O_2Se$ requires (%): C 41.81, H 3.03. ^{1}H NMR (d_6-DMSO), δ 8.03 [dd, 1H, Ar–H(6), *J* 7.72, 1.36], 7.67 [d, 1H, Ar–H(3), *J* 7.88], 7.48 [dt, 1H, Ar–H(4), *J* 8.24, 1.36], 7.35 [t, 1H, Ar–H(5), *J* 7.68]. $^{13}C\{^1H\}$ NMR, δ 169.10 (C7), 134.03 (C2), 133.91 (C3), 132.05 (C4), 129.93 (C1), 129.32 (C6), 127.00 (C5). FTIR (cm^{-1}): 3437(m), 3061(w), 2662(w), 2562(w), 1672(s), 1584(w), 1559(w), 1459(m), 1432(w), 1415(w), 1310(w), 1285(m), 1264(s), 1148(m), 1027(m), 903(w), 804(w), 738(m), 679(w), 644(w), 550(w).

Synthesis of $[Pt(SeC_6H_4CO_2)(PPh_3)_2]$ 4a

Selenosalicylic acid **2** (25.4 mg, 0.127 mmol) was added to a mixture of *cis*-$[PtCl_2(PPh_3)_2]$ (100 mg, 0.126 mmol) and triethylamine (5 drops) in methanol (15 mL). The mixture was refluxed for 2 h and cooled to room temperature. Water (30 mL) was then added to isolate the neutral complex as a yellow solid. This was purified by recrystallising from dichloromethane (5 mL): petroleum spirit (7 mL). Yield 68 mg (58%). M.p. 154–156 °C. Found (%): C 56.04, H 3.79; $C_{43}H_{34}O_2P_2PtSe$ requires (%): C 56.21, H 3.73. $^{31}P\{^1H\}$ NMR, δ 21.5 (d, $^1J_{Pt-P}$ 2897, $^2J_{P-P}$ 19, $^2J_{P-Se}$ 49), 7.2 (d, $^1J_{Pt-P}$ 3917, $^2J_{P-P}$ 19, $^2J_{P-Se}$ 27). ^{1}H NMR, δ 7.74 (q, 2H,

Ar–H, *J* 5.92), 7.69 (dd, 1H, Ar–H, *J* 7.56, 1.24), 7.54 (dd, 4H, Ar–H, *J* 11.88, 7.56), 7.32–7.46 (m, 16H, Ar–H), 7.15–7.24 (tt, 9H, Ar–H, *J* 11.00 2.44), 7.10 (t, 1H, Ar–H, *J* 7.32), 7.02 (td, 1H, Ar–H, *J* 7.48, 1.48). FTIR (cm^{-1}): 3052 (w), 2918(w), 2850(w), 1621(s), 1583(m), 1481(m), 1435(s), 1320(s), 1185(w), 1138(w), 1096(s), 1028(w), 998(w), 857(w), 743(s), 692(s), 549(s), 525(s), 460(w).

The following complexes were prepared using the same general procedure as for **4a**.

Synthesis of $[Pd(SeC_6H_4CO_2)(PPh_3)_2]$ 4b

$[PdCl_2(PPh_3)_2]$ (100 mg, 0.143 mmol) was mixed with **2** (28.7 mg, 0.143 mmol) and triethylamine (5 drops) in a flask and refluxed for 2 h, resulting in an orange coloured product. Yield 66 mg (66%). M.p. 122–124 °C. Found (%): C 61.92, H 4.28; $C_{43}H_{34}O_2P_2PdSe$ requires (%): C 62.22, H 4.13. $^{31}P\{^1H\}$ NMR, δ 32.9 (d, $^2J_{P-P}$ 30), 18.4 (d, $^2J_{P-P}$ 30). ^1H NMR, δ 7.54 (dd, 6H, Ar–H, *J* 11.44, 7.92), 7.38 (dd, 3H, Ar–H, *J* 8.00, 6.52), 7.29–7.35 (m, 11H, Ar–H), 7.21 (td, 6H, Ar–H, *J* 7.84, 2.28), 7.13 (td, 6H, Ar–H, *J* 7.96, 2.04), 7.02 (dt, H, Ar–H, *J* 7.20). FTIR (cm^{-1}): 3054(w), 2918(w), 2850(w), 1614(s), 1594(s), 1547(w), 1480(m), 1435(s), 1330(m), 1186(w), 1141(w), 1096(w), 1027(w), 998(w), 850(w), 742(s), 693(s), 537(s), 521(s).

Synthesis of $[Pd(SeC_6H_4CO_2)(dppe)]$ 4c

Complex **4c** was obtained as an orange solid by reacting $[PdCl_2(dppe)]$ (100 mg, 0.174 mmol) and **2** (34.9 mg, 0.174 mmol) with added triethylamine (5 drops). Yield 75 mg (61%). M.p. 152–155 °C. Found (%): 56.14, H 4.02; $C_{33}H_{28}O_2P_2PdSe$ requires (%): C 56.31, H 4.01. $^{31}P\{^1H\}$ NMR, δ 58.1 (d, $^2J_{P-P}$ 27), 39.7 (d, $^2J_{P-P}$ 27). ^1H NMR, δ 7.94 (m, 5H, Ar–H), 7.78 (dd, 4H, *J* 12.44, 7.24), 7.49–7.59 (m, 13H, Ar–H), 7.12 (t, 1H, Ar–H, *J* 7.16), 7.02 (td, 1H, Ar–H, *J* 7.64, 1.4), 2.23 (m, 2H, CH_2 {dppe}), 2.51 (m, 2H, CH_2 {dppe}). FTIR (cm^{-1}): 3052 (w), 2918(w), 2850(w), 1592(s), 1582(s), 1483(w), 1435(s), 1342(m), 1187(w), 1103(m), 1027(w), 998(w), 878(w), 849(w), 821(w), 745(s), 716(s), 705(s), 690(s), 531(s), 489(w).

Synthesis of $[Pd(SeC_6H_4CO_2)(phen)]$ 4d

A mixture of $[PdCl_2(phen)]$ (100 mg, 0.280 mmol) was refluxed with **2** (56.2 mg, 0.280 mmol) and triethylamine (5 drops) in methanol (15 mL) and purified as for **4a** to give a brown solid of **4d**. Yield 55 mg (40%). M.p. 176–178 °C. Found (%): 46.10, H 2.88, N 5.81; $C_{19}H_{12}N_2O_2PdSe$ requires (%): C 46.98, H 2.49, N 5.77. ^1H NMR, δ 9.32 (d, 1H, Ar–H, *J* 4.84), 9.15 (d, 1H, Ar–H, *J* 5.04), 8.57 (d, 1H, Ar–H, *J* 8.24), 8.51 (d, 1H, Ar–H, *J* 7.96), 8.14 (d, 1H, Ar–H, *J* 7.88), 7.95 (m, 3H, Ar–H), 7.77 (dd, 1H, Ar–H, *J* 8.12, 5.44), 7.69 (d, 1H, Ar–H, *J* 7.52), 7.14–7.22 (m, 2H, Ar–H). FTIR (cm^{-1}): 2918(w), 2850(w), 1629(m), 1582(s), 1516(m), 1428(m), 1383(s), 1146(w), 1108(w), 874(w), 847(m), 752(m), 716(s).

Synthesis of $[Pd(SeC_6H_4CO_2)(dppf)]$ 4e

Reaction of $[PdCl_2(dppf)]$ (100 mg, 0.137 mmol), **2** (27.5 mg, 0.137 mmol) and triethylamine (5 drops) gave **4e** as a brown solid. Yield 61 mg (52%). M.p. 175–178 °C. Found (%): C 54.93, H 4.16; $C_{41}H_{32}FeO_2P_2PdSe$ requires (%): C 54.97, H 4.05. $^{31}P\{^1H\}$ NMR, δ 23.6 (d, $^2J_{P-P}$ 27), 15.8 (d, $^2J_{P-P}$ 24). ^1H NMR, δ 7.94 (dd, H, Ar–H, *J* 10.52), 7.70 (dd, H, Ar–H, *J* 12.48, 8.24), 7.33–7.54 (m, H, Ar–H), 6.98 (dt, H, Ar–H, *J* 7.00), 4.76 (s, 2H, CH {dppf}), 4.52 (s, 2H, CH {dppf}), 4.30 (s, 2H, CH {dppf}), 3.76 (s, 2H, CH {dppf}). FTIR (cm^{-1}): 3053(w), 2921(w), 2851(w), 1613(s), 1592(s), 1546(m), 1481(w), 1435(s), 1384(w), 1347(m), 1166(m), 1097(m), 1028(m), 998(w), 848(w), 824(w), 744(s), 694(s), 637(w), 551(m), 526(w), 512(w), 491(m), 467(w).

Synthesis of $[Ni(SeC_6H_4CO_2)(dppe)]$ 4f

Reaction of $[NiCl_2(dppe)]$ (100 mg, 0.190 mmol), **2** (38.1 mg, 0.190 mmol), and triethylamine (5 drops) gave **4f** as an orange solid. Yield 81 mg (65%). M.p. 133–136 °C. Found (%): C 60.64, H 4.13; $C_{33}H_{28}NiO_2P_2Se$ requires (%): C 60.40, H 4.30. $^{31}P\{^1H\}$-NMR (162 MHz): δ 57.29 (d, $^2J_{P-P}$ 51, $^2J_{P-Se}$ 51), 40.23 (d, $^2J_{P-P}$ 51 Hz, $^2J_{P-Se}$ 50). ^1H-NMR (400 MHz, δ): 8.05 (m, 4H, Ar–H), 7.94 (dd, 4H, Ar–H, $J = 10.68$, 8.20 Hz), 7.52 (m, 14H, Ar–H), 7.11 (t, 1H, Ar–H, $J = 7.12$ Hz), 7.01 (t, 1H, Ar–H, $J = 7.24$ Hz), 2.02 (m, 2H, CH_2 {dppe}), 2.36 (m, 2H, CH_2 {dppe}). FTIR (cm^{-1}): 3052(w), 2917(w), 2850(w), 1598(s), 1582(s), 1545(m), 1483(m), 1453(w), 1435(s), 1335(s), 1276(w), 1187(w), 1144(w), 1101(m), 1027(m), 998(m), 876(w), 819(m), 744(s), 716(s), 703(s), 690(s), 656(w), 532(s), 486(m).

Synthesis of $[\{Pd(bipy)\}_2(Cl)(SeC_6H_4CO_2)]Cl$ 4g

Complex **4g** was obtained as a brown solid by refluxing $[PdCl_2(bipy)]$ (100 mg, 0.3 mmol) with **2** (60.3 mg, 0.3 mmol) and triethylamine (5 drops) in methanol (15 mL). Yield 100 mg (44%). M.p. 162–164 °C. Found (%): C 42.40, H 2.95, N 7.61; $C_{27}H_{20}ClN_4O_2Pd_2Se$ requires (%): C 42.68, H 2.65, N 7.37. ^1H NMR, δ 9.12 (d, 2H, Ar–H, *J* 5.2), 8.76 (d, 1H, Ar–H, *J* 5.00), 8.65 (d, 1H, Ar–H, *J* 5.52), 8.56 (m, 4H, Ar–H), 8.30–8.40 (m, 4H, Ar–H), 7.96 (t, 1H, Ar–H, *J* 12.92), 7.80 (t, 3H, Ar–H, *J* 7.16), 7.71 (t, 1H, Ar–H, *J* 6.76), 7.55 (t, 1H, Ar–H, *J* 4.84), 7.11 (t, 2H, Ar–H, *J* 4.32). $^{13}C\{^1H\}$ NMR, δ 169.91, 157.68, 156.88, 154.13, 151.69, 150.16, 145.49, 141.70, 141.46, 141.32, 133.21, 131.93, 130.13, 129.62, 128.29, 127.91, 127.77, 124.86, 124.34, 123.71. FTIR (cm^{-1}): 3105(w), 3074(w), 2919(w), 2850(w), 1599(s), 1573(w), 1542(s), 1494(w), 1467(m), 1446(w), 1430(m), 1360(s), 1311(w), 1276(w), 1248(w), 1163(w), 1146(w), 1106(w), 1071(w), 1035(w), 866(w), 765(s), 722(s), 664(w), 647(w), 507(w), 481(w).

Synthesis of $[(p\text{-cym})Ru(SeC_6H_4CO_2)(PPh_3)]$ 4h

The complex **4h** was synthesised when $[(p\text{-cym})RuCl_2(PPh_3)]$ (70 mg, 0.123 mmol) was refluxed with **2** (24.8 mg, 0.123 mmol) and triethylamine (5 drops) in methanol (10 mL). Yield 55 mg (41%). M.p. 104–106 °C. Found (%): C 60.27, H 4.79; $C_{35}H_{33}O_2PRuSe$ requires (%): C 60.34, H 4.77. $^{31}P\{^1H\}$ NMR, δ 35.5 (s). ^1H NMR, δ 7.86 (dd, 1H, Ar–H, *J* 7.68, 1.32), 7.62 (m, 10H, Ar–H), 7.40 (m, 6H, Ar–H), 7.06 (dt, 1H, Ar–H, *J* 7.64, 1.12), 6.96 (dt, 1H, Ar–H, *J* 7.52, 1.56), 5.36 (d, 1H, Ar–H {*p*-cym}, *J* 6.08), 5.09 (d, 1H, Ar–H {*p*-cym}, *J* 5.96), 4.85 (d, 1H, Ar–H {*p*-cym}, *J* 6.04), 4.45 (d, 1H, Ar–H {*p*-cym}, *J* 5.72), 2.45 (hept, 1H, $CHMe_2$ {*p*-cym}, *J* 6.92), 1.97 (s, 3H, Me {*p*-cym}), 1.18 (d, 3H, $CHMe_A$ {*p*-cym}, *J* 6.88), 1.07 (d, 3H, $CHMe_B$ {*p*-cym}, *J* 6.96). FTIR (cm^{-1}): 3052(w),

2960(w), 2919(w), 2867(w), 1591(s), 1545(m), 1481(m), 1435(s), 1345(m), 1187(w), 1093(m), 1028(m), 853(w), 801(w), 745(s), 697(s), 526(s), 511(m), 499(w).

Synthesis of $[(C_6Me_6)Ru(SeC_6H_4CO_2)(PPh_3)]$ 4i

$[(C_6Me_6)RuCl_2(PPh_3)]$ (27 mg, 0.045 mmol) was refluxed with **2** (9.1 mg, 0.045 mmol) and triethylamine (3 drops) in methanol (10 mL) for 2 h, and the reaction mixture was worked up as for **4a** to give a brown solid of **4i**. Yield 20 mg (61%). M.p. 114–117 °C. Found (%): C 61.54, H 4.94; $C_{37}H_{37}O_2PRuSe$ requires (%): C 61.32, H 5.15. $^{31}P\{^1H\}$ NMR, δ 29.4 (s). ^1H NMR, δ 8.12 (d, 1H, Ar–H, *J* 7.20), 7.76 (d, 1H, Ar–H, *J* 7.40), 7.56 (t, 1H, Ar–H, *J* 7.40), 7.49 (m, 3H, Ar–H), 7.35–7.41 (m, 12H, Ar–H), 7.17 (t, 1H, Ar–H, *J* 7.20), 1.70 (s, 18H, CH_3 {C_6Me_6}). FTIR (cm^{-1}): 3055(w), 2918(w), 2850(w), 1614(s), 1602(s), 1453(w), 1436(w), 1384(w), 1336(s), 1142(w), 1069(w), 1026(w), 848(w), 750(m), 722(w), 697(w), 542(w), 498(w).

Synthesis of $[Cp^*Rh(SeC_6H_4CO_2)(PPh_3)]$ 4j

A red solid of **4j** was obtained from a refluxing mixture of $[Cp^*RhCl_2(PPh_3)]$ (60 mg, 0.105 mmol), **2** (21.1 mg, 0.105 mmol), and triethylamine (3 drops) in methanol (10 mL). Yield 30 mg (41%). M.p. 127–130 °C. Found (%): C 59.95, H 4.86; $C_{35}H_{34}O_2PRhSe$ requires (%): C 60.10, H 4.90. $^{31}P\{^1H\}$ NMR, δ 34.0 (d, $^1J_{Rh-P}$ 150). ^1H NMR, δ 7.86 (d, 1H, Ar–H, *J* 7.56), 7.62 (t, 6H, Ar–H, *J* 8.28 Hz), 7.50 (d, 1H, Ar–H, *J* 7.48), 7.40 (m, 10H, Ar–H), 7.00 (t, 1H, Ar–H, *J* 7.16), 6.92 (t, 1H, Ar–H, *J* 7.40), 1.27 (s, 15H, CH_3 {Cp*}). FTIR (cm^{-1}): 3052(w), 2917(w), 2850(w), 1583(s), 1566(s), 1536(s), 1481(w), 1435(m), 1358(m), 1157(m), 1095(m), 1029(m), 744(s), 700(s), 526(s), 510(m), 496(w).

Synthesis of $[Cp^*Ir(SeC_6H_4CO_2)(PPh_3)]$ 4k

$[Cp^*Ir(SeC_6H_4CO_2)(PPh_3)]$ was isolated as a yellow solid from a refluxed mixture of $[Cp^*IrCl_2(PPh_3)]$ (50 mg, 0.0756 mmol), **2** (15.2 mg, 0.0756 mmol) and triethylamine (3 drops) in methanol, followed by workup as for **4a**. Yield 34 mg (57%). M.p. 124–126 °C. Found (%): C 53.27, H 4.26; $C_{35}H_{34}IrO_2PSe$ requires (%): C 53.29, H 4.34. $^{31}P\{^1H\}$ NMR, δ 7.5 (s). ^1H NMR, δ 7.86 (d, 1H, Ar–H, *J* 7.72), 7.57 (t, 6H, Ar–H, *J* 8.16), 7.46 (d, 1H, Ar–H, *J* 7.52), 7.40 (m, 10H, Ar–H), 6.99 (t, 1H, Ar–H, *J* 7.24), 6.90 (dt, 1H, Ar–H, *J* 7.52, 1.28), 1.28 (s, 15H, CH_3 {Cp*}). FTIR (cm^{-1}): 3053(w), 2917(w), 2850(w), 1612(s), 1592(s), 1545(m), 1482(w), 1435(m), 1376(w), 1336(m), 1134(w), 1097(m), 1029(m), 853(w), 744(m), 700(s), 533(s), 512(m).

Synthesis of $[\{Cp^*Rh(SeC_6H_4CO_2)\}_2]$ 4l

The neutral dimeric complex **4l** was obtained by refluxing $[Cp^*RhCl_2]_2$ (100 mg, 0.162 mmol), **2** (65 mg, 0.324 mmol), and triethylamine (5 drops) in methanol (15 mL) for 2 h. Water (30 mL) was then added to the brownish-red solution and was left to crystallise as red microcrystals after 2 days. Yield 150 mg (53%). M.p. >285 °C (decomp.). Found (%): C 46.65, H 4.35; $C_{34}H_{38}O_4Rh_2Se_2$ requires (%): C 46.70, H 4.38. ^1H NMR, δ 8.21 (dd, 2H, Ar–H, *J* 7.72, 1.24), 7.69 (d, 2H, Ar–H, *J* 6.84), 7.35 (td, 2H, Ar–H, *J* 7.68, 1.00), 7.18 (td, 2H, Ar–H, *J* 7.44, 1.40), 1.34 (s, 30H, CH_3 {Cp*}). $^{13}C\{^1H\}$ NMR, δ 171.0, 139.95, 135.08, 133.37, 128.57, 128.21, 126.65, 94.99, 8.68. FTIR (cm^{-1}): 2918(w), 2850(w), 1634(m), 1588(s), 1551(m), 1453(w), 1383(w), 1353(m), 1160(w), 1029(w), 847(w), 765(m).

Synthesis of $[(bp)Au(SeC_6H_4CO_2)]$ 4m

Complex **4m** was prepared by adding selenosalicylic acid **2** (46.1 mg, 0.229 mmol) to a stirred methanolic (15 mL) suspension of benzylpyridylgold(III) chloride (100 mg, 0.229 mmol) in a flask covered with aluminum foil and placed in the dark, followed by the addition of triethylamine (5 drops). The mixture was stirred for 1 h and water (30 mL) was added to precipitate the product as a greenish-yellow solid. Yield 84.8 mg (65%). M.p. 158–160 °C. Found (%): 40.71, H 2.51, N 2.32; $C_{19}H_{14}AuNO_2Se$ requires (%): C 40.44, H 2.50, N 2.48. ^1H NMR, δ 9.16 (d, 1H, Ar–H, *J* 5.68), 8.19 (dd, 1H, Ar–H, *J* 7.68, 1.80), 8.00 (td, 1H, Ar–H, *J* 7.68, 1.48), 7.62–7.69 (m, 3H, Ar–H), 7.55 (d, 1H, Ar–H, *J* 7.76 Hz), 7.21–7.28 (m, 3H, Ar–H), 7.09 (m, 2H, Ar–H), 4.30 (s, 2H, CH_2). $^{13}C\{^1H\}$ NMR, δ 170.13, 154.83, 152.19, 148.60, 142.24, 141.49, 137.65, 134.36, 134.05, 133.48, 131.19, 130.08, 129.06, 128.44, 128.12, 126.13,125.36, 124.61, 47.66. FTIR (cm^{-1}): 3078(w), 2917(w), 2850(w), 1595(s), 1579(s), 1550(m), 1484(w), 1461(w), 1426(m), 1349(s), 1294(w), 1160(w), 1145(w), 1102(w), 1051(w), 1029(m), 862(w), 833(w), 754(s), 711(w), 620(m), 575(w), 477(w).

Synthesis of $[(PPh_3Au)_2(SeC_6H_4CO_2)]$ 4n

Ph_3PAuCl (100 mg, 0.202 mmol) was suspended in ethanol (15 mL) and NaOH (0.203 mmol, 2 mL of a 0.1 M solution) was added, followed by **2** (40.6 mg, 0.202 mmol), and the mixture was stirred for 30 min. at room temperature to give a clear, light-yellow solution. This was filtered and the filtrate was left to evaporate over 3 days, resulting in a light yellow solid of **4n**. Yield 100 mg (44%). M.p. 126–129 °C. Found (%): C 46.12, 3.01; $C_{43}H_{34}Au_2O_2P_2Se$ requires (%): C 46.21, H 3.07. $^{31}P\{^1H\}$ NMR (d_6-DMSO), δ 35.6 (s), δ 25.6 (s). ^1H NMR, δ 7.92 (dd, 1H, Ar–H, *J* 8.64, 1.68), 7.87 (t, 1H, Ar–H, *J* 4.36), 7.53–7.66 (m, 27H, Ar–H), 7.38 (dd, 1H, Ar–H, *J* 6.84, 2.16), 7.09 (t, 2H, Ar–H, *J* 4.44), 7.02 (t, 2H, Ar–H, *J* 6.80). FTIR (cm^{-1}): 3436(br, s) 3051(w), 2918(w), 2850(w), 1636(m), 1583(s), 1546(m), 1480(m), 1435(s), 1383(m), 1254(w), 1100(s), 1026(m), 997(m), 795(w), 744(s), 710(w), 692(s), 535(s), 508(m).

X-ray crystallographic analyses

Crystals of the complexes were obtained by slow diffusion of diethyl ether into dichloromethane solutions. In the case of complex **4h′**, crystals were obtained from an attempt to grow crystals of the phosphine derivative **4h**. X-ray diffraction data for **4a** and **4l** were collected at 140 K while those of **4h′** and **4k** were collected at 100 K on an Agilent SuperNova, Single source at offset, Atlas diffractometer with graphite-monochromated Cu–K_α radiation and corrected for absorption using a multi-scan procedure.[87] The structures were solved with the Olex2.solve[88] structure solution program on Olex2 [89] using Charge Flipping and refined with the Olex2.refine[88] refinement package using Gauss-Newton minimisation. The ligand of **4a** is disordered

with the positions of the selenium and carboxylate atoms each occupying two sites, and was modelled with occupancies of 90 and 10%. Also, the carbon and one oxygen atom of the carboxylate group of the minor orientation, C7B and O2B, were refined with isotropic thermal displacement. This is repeated in **4k** where the Se and carboxylate atoms are modelled with occupancies of 65 and 35%, and one ligand oxygen of the minor orientation, O2C, is virtually coincident with the selenium atom of the major orientation, Se1B, necessitating its refinement with isotropic thermal displacement.

Hirshfeld surface analysis

The crystal structure packings of **4h′** and **4k** were generated from the CIF files and quantified with Hirshfeld surface analysis and the associated 2D-fingerprint plots using CrystalExplorer package.[90]

Conflicts of interest

There are no conflicts to declare.

Acknowledgements

We thank the University of Waikato for financial support of this work, Dr Judith Burrows for X-ray data collection, and Jenny Stockdill for technical assistance. S. A. thanks the Tertiary Education Trust Fund (TETfund) Nigeria for financial support.

References

1 T. Wehr-Candler and W. Henderson, *Coord. Chem. Rev.*, 2016, **313**, 111–155.
2 A. P. Fernandes and V. Gandin, *Biochim. Biophys. Acta, Gen. Subj.*, 2015, **1850**, 1642–1660.
3 K. A. Cupp-Sutton and M. T. Ashby, *Antioxidants*, 2016, **5**, 42.
4 A. V. Lobanov, D. L. Hatfield and V. N. Gladyshev, *Biochim. Biophys. Acta*, 2009, **1790**, 1424–1428.
5 F. Gorini, L. Sabatino, A. Pingitore and C. Vassalle, *Molecules*, 2021, **26**, 7084.
6 Z. L. Cai, J. Z. Zhang and H. J. Li, *Aging: Clin. Exp. Res.*, 2019, **31**, 1035–1047.
7 S. Hariharan and S. Dharmaraj, *Inflammopharmacology*, 2020, **28**, 667–695.
8 M. Roman, P. Jitaru and C. Barbante, *Metallomics*, 2014, **6**, 25–54.
9 G. Barchielli, A. Capperucci and D. Tanini, *Antioxidants*, 2022, **11**, 251.
10 C. W. Nogueira, N. V. Barbosa and J. B. T. Rocha, *Arch. Toxicol.*, 2021, **95**, 1179–1226.
11 K. P. Bhabak and G. Mugesh, *Acc. Chem. Res.*, 2010, **43**, 1408–1419.
12 E. R. T. Tiekink, *Dalton Trans.*, 2012, **41**, 6390–6395.
13 Y. Liu, L. Li, H.-Y. Zhang and Y. Song, *J. Org. Chem.*, 2003, **68**, 527–536.
14 L. Engman, D. Stern, H. Frisell, K. Vessman, M. Berglund, B. Ek and C. M. Andersson, *Bioorg. Med. Chem.*, 1995, **3**, 1255–1262.
15 J. Malmstrom, M. Jonsson, I. A. Cotgreave, L. Hammarstrom, M. Sjodin and L. Engman, *J. Am. Chem. Soc.*, 2001, **123**, 3434–3440.
16 T. Fenner and C. H. Schiesser, *Molecules*, 2004, **9**, 472–479.
17 M. A. Lucas, O. T. K. Nguyen, C. H. Schiesser and S. L. Zheng, *Tetrahedron*, 2000, **56**, 3995–4000.
18 T. G. Back and Z. Moussa, *J. Am. Chem. Soc.*, 2003, **125**, 13455–13460.
19 T. G. Back and Z. Moussa, *J. Am. Chem. Soc.*, 2002, **124**, 12104–12105.
20 M. Carland and T. Fenner, The Use of Selenium-Based Drugs in Medicine, in *Metallotherapeutic Drugs and Metal-Based Diagnostic Agents: The Use of Metals in Medicine*, John Wiley and Sons Limited, 2005, pp. 313–332.
21 H. E. Ganther and J. R. Lawrence, *Tetrahedron*, 1997, **53**, 12299–12310.
22 G. Mugesh, W. W. du Mont and H. Sies, *Chem. Rev.*, 2001, **101**, 2125–2179.
23 S. W. May, *Expert Opin. Invest. Drugs*, 1999, **8**, 1017–1030.
24 M. Rooseboom, G. Schaaf, J. N. Commandeur, N. P. Vermeulen and J. Fink-Gremmels, *J. Pharmacol. Exp. Ther.*, 2002, **301**, 884–892.
25 M. Koketsu, H. Ishihara and M. Hatsu, *Res. Commun. Chem. Pathol. Pharmacol.*, 1998, **101**, 179–186.
26 L. Dupont, O. Dideberg and P. Jacquemin, *Acta Crystallogr., Sect. C: Cryst. Struct. Commun.*, 1990, **46**, 484–486.
27 K. P. Bhabak and G. Mugesh, *Chem.–Eur. J.*, 2007, **13**, 4594–4601.
28 B. J. Bhuyan and G. Mugesh, *Org. Biomol. Chem.*, 2011, **9**, 1356–1365.
29 O. R. Tamtaji, R. Heidari-Soureshjani, N. Mirhosseini, E. Kouchaki, F. Bahmani, E. Aghadavod, M. Tajabadi-Ebrahimi and Z. Asemi, *Clin. Nutr.*, 2019, **38**, 2569–2575.
30 C. J. Dong, J. Wang, H. Chen, P. Wang, J. X. Zhou, Y. Zhao and L. L. Zou, *Metallomics*, 2020, **12**, 860–867.
31 E. S. Çetin, M. Naziroğlu, B. Çiğ, I. S. Övey, P. A. Koşar and J. Receptor, *Signal Transduction*, 2017, **37**, 84–93.
32 R. Mamgain and F. V. Singh, *ACS Org. Inorg. Au*, 2022, **2**, 262–288.
33 S. Ramos-Inza, P. Daniel and S. Carmen, *Eur. J. Med. Chem.*, 2022, **244**, 114834.
34 J. Ashaks, Y. Bankovsky, D. Zaruma, I. Shestakova, I. Domracheva, A. Nesterova and E. Lukevics, *Chem. Heterocycl. Compd.*, 2004, **40**, 776–780.
35 L. B. Kumbhare, V. K. Jain, P. P. Phadnis and M. Nethaji, *J. Organomet. Chem.*, 2007, **692**, 1546–1556.
36 R. S. Chauhan, R. K. Sharma, G. Kedarnath, D. B. Cordes, A. M. Slawin and V. K. Jain, *J. Organomet. Chem.*, 2012, **717**, 180–186.
37 P. G. Jones and C. Thöne, *Chem. Rep.*, 1990, **123**, 1975–1978.
38 J. Kampf, R. Kumar and J. P. Oliver, *Inorg. Chem.*, 1992, **31**, 3626–3629.
39 L. Rummel, G. Lassandro, M. Seidl, A. Y. Timoshkin and M. Scheer, *Dalton Trans.*, 2021, **50**, 12648–12654.
40 I. Zwolak, *Biol. Trace Elem. Res.*, 2020, **193**, 44–63.
41 A. S. Rahmanto and M. J. Davies, *IUBMB life*, 2012, **64**, 863–871.

42 R. Huber and R. Criddle, *Arch. Biochem. Biophys.*, 1967, **122**, 164–173.
43 R. Gusmao, R. Prohens, J. M. Díaz-Cruz, C. Arino and M. Esteban, *J. Biol. Inorg. Chem.*, 2012, **17**, 321–329.
44 K. M. Williams, R. P. Dudgeon, S. C. Chmely and S. R. Robey, *Inorg. Chim. Acta*, 2011, **368**, 187–193.
45 G. Faraglia, D. Fregona and S. Sitran, *Transition Met. Chem.*, 1997, **22**, 492–496.
46 A. Panneerselvam, C. Q. Nguyen, J. Waters, M. A. Malik, P. O'Brien, J. Raftery and M. Helliwell, *Dalton Trans.*, 2008, **33**, 4499–4506.
47 P. Sarkar, T. J. Konch, T. Kamilya, K. Raidongia, S. Acharya and C. Mukherjee, *Chem. Commun.*, 2020, **56**, 15220–15223.
48 S. Keimatsu, K. Yokota and I. Satoda, *Yakugaku Zasshi*, 1932, **52**, 531–542.
49 B. Boettcher, W. R. Walker and M. W. Whitehouse, *US Pat.*, 4287190A, 1981.
50 B. Boettcher, W. R. Walker and M. W. Whitehouse, *EP Pat.*, 2341A1, 1979.
51 For selected recent reviews seeR. S. Chauhan, *New J. Chem.*, 2020, **44**, 2689–2696; V. K. Jain, *New J. Chem.*, 2019, **43**, 11034–11040.
52 C. G. Wilber, *Clin. Toxicol.*, 1980, **17**, 171–230.
53 N. Kamigata, H. Iizuka, A. Izuoka and M. Kobayashi, *Bull.Chem.Soc.Jpn*, 1986, **59**, 2179–2183.
54 C. Allen and D. MacKay, *Org. Synth.*, 1932, **12**, 76.
55 L. J. McCaffrey, W. Henderson, B. K. Nicholson, J. E. Mackay and M. B. Dinger, *J. Chem. Soc., Dalton Trans.*, 1997, 2577–2586.
56 W. Henderson, B. K. Nicholson, A. G. Oliver and C. E. F. Rickard, *J. Organomet. Chem.*, 2001, **625**, 40–46.
57 M. B. Dinger and W. Henderson, *J. Organomet. Chem.*, 1998, **560**, 233–243.
58 W. Henderson, B. K. Nicholson, S. J. Faville, D. Fan and J. D. Ranford, *J. Organomet. Chem.*, 2001, **631**, 41–46.
59 S. D. J. Brown, W. Henderson, K. J. Kilpin and B. K. Nicholson, *Inorg. Chim. Acta*, 2007, **360**, 1310–1315.
60 K. Nomiya, N. C. Kasuga, I. Takamori and K. Tsuda, *Polyhedron*, 1998, **17**, 3519–3530.
61 W. Henderson, J. C. Thomas, O. C. Okpareke and E. R. T. Tiekink, *Inorg. Chim. Acta*, 2019, **490**, 104–111.
62 N. J. Rijs and R. A. J. O'Hair, *Dalton Trans.*, 2012, **41**, 3395–3406.
63 R. L. Cunha, I. E. Gouvea and L. Juliano, *Annals Brazil. Acad. Sci.*, 2009, **81**, 393–407.
64 W. Henderson, L. J. McCaffrey and B. K. Nicholson, *J. Chem Soc., Dalton Trans.*, 2000, 2753–2760.
65 A. Sladek, W. Schneider, K. Angermaier, A. Bauer and H. Schmidbaur, *Z. Naturforsch.*, 1996, **51B**, 765–772.
66 D. De Vos, P. Clements, S. M. Pyke, D. R. Smyth and E. R. T. Tiekink, *Met.-Based Drugs*, 1999, **6**, 31–40.
67 T. B. Schroeder, C. Job, M. F. Brown and R. S. Glass, *Magn. Reson. Chem.*, 1995, **33**, 191–195.
68 D. L. Davies, J. Fawcett, R. Krafczyk, D. R. Russell and K. Singh, *J. Chem. Soc., Dalton Trans.*, 1998, 2349–2352.
69 L. Battan, S. Fantasia, M. Manassero, A. Pasini and M. Sansoni, *Inorg. Chim. Acta*, 2005, **358**, 555–564.
70 L. Fuks, E. Gniazdowska and P. Koźmiński, *Polyhedron*, 2010, **29**, 634.
71 K. Nomiya, H. Yokoyama, H. Nagano, M. Oda and S. Sakuma, *J. Inorg. Biochem.*, 1989, **60**, 289.
72 S. Suda, A. Tateno, D. Nakane and T. Akitsu, *Int. J. Org. Chem.*, 2023, **13**, 57–85.
73 I. Feddaoui, M. S. Abdelbaky, S. García-Granda, K. Essalah, C. B. Nasr and M. L. Mrad, *J. Mol. Struct.*, 2019, **1186**, 31–38.
74 Y. Laamari, M. Fawzi, M. E. Hachim, A. Bimoussa, A. Oubella, E. M. Ketatni, M. Saadi, L. El Ammari, M. Y. Itto, H. Morjani and M. Khouili, *J. Mol. Struct.*, 2024, **1297**, 136864.
75 D. Drew and J. R. Doyle, *Inorg. Synth.*, 1972, **13**, 52–53.
76 J. X. McDermott, J. F. White and G. M. Whitesides, *J. Am. Chem. Soc.*, 1976, **98**, 6521–6528.
77 D. L. Oliver and G. K. Anderson, *Polyhedron*, 1992, **11**, 2415–2420.
78 B. J. McCormick, E. N. Jaynes Jr and R. I. Kaplan, *Inorg. Synth.*, 1972, **13**, 216.
79 F. L. Wimmer, S. Wimmer and P. Castan, *Inorg. Synth.*, 1992, **29**, 185.
80 G. R. Van Hecke and W. D. Horrocks Jr, *Inorg. Chem.*, 1966, **5**, 1968.
81 P. Štěpnička, R. Gyepes, O. Lavastre and P. H. Dixneuf, *Organometallics*, 1997, **16**, 5089–5095.
82 J. W. Kang, K. Moseley and P. M. Maitlis, *J. Am. Chem. Soc.*, 1969, **91**, 5970.
83 B. L. Booth, R. N. Haszeldine and M. Hill, *J. Organomet. Chem.*, 1969, **16**, 491–496.
84 R. Sáez, J. Lorenzo, M. J. Prieto, M. Font-Bardia, T. Calvet, N. Omeñaca, M. Vilaseca and V. Moreno, *J. Inorg. Biochem.*, 2014, **136**, 1–12.
85 M. A. Cinellu, A. Zucca, S. Stoccoro, G. Minghetti, M. Manassero and M. Sansoni, *J. Chem. Soc., Dalton Trans.*, 1995, 2865–2872.
86 M. Bruce, B. Nicholson, O. B. Shawkataly, J. Shapley and T. Henly, *Inorg. Synth.*, 1989, **26**, 324–328.
87 R. H. Blessing, *Acta Crystallogr.*, 1995, **A51**, 33–38.
88 L. J. Bourhis, O. V. Dolomanov, R. J. Gildea, J. A. K. Howard and H. Puschmann, *Acta Crystallogr.*, 2015, **A71**, 59–75.
89 O. V. Dolomanov, L. J. Bourhis, R. J. Gildea, J. A. K. Howard and H. Puschmann, *J. Appl. Crystallogr.*, 2009, **42**, 339–341.
90 P. R. Spackman, M. J. Turner, J. J. McKinnon, S. K. Wolff, D. J. Grimwood, D. Jayatilaka and M. A. Spackman, *J. Appl. Crystallogr.*, 2021, **54**, 1006–1011.